

Cold gas in the Perseus cluster core: Excitation of molecular gas in filaments

Salomé, P.^{1,*}, Combes, F.², Revaz Y.², Edge A.C.³, Hatch N.A.⁵, Fabian A.C.⁴, and Johnstone R.M.⁴

¹ Institut of Radio Astronomy (IRAM), Domaine Universitaire, 300, rue de la piscine, F-38400 St Martin d'Hères, France
e-mail: salome@iram.fr

² Observatoire de Paris, LERMA, 61 Av. de l'Observatoire, F-75014, Paris, France

³ Department of Physics, University of Durham, South Road, Durham DH1 3LEi, UK

⁴ Institute of Astronomy, Madingley Road, Cambridge CB3 0HA, UK

⁵ Leiden Observatory, NL-2300 RA Leiden, The Netherlands

Received 4 February 2008 / Accepted 14 March 2008

Abstract. We have recently detected CO lines in the well-known filaments around NGC 1275, the galaxy at the centre of the Perseus cluster of galaxies. These previous observations, with the HERA multi-beam array at the IRAM 30m telescope enabled us to make a large map of the CO(2–1) line and to see hints of molecular gas far away from the cluster centre. To confirm the presence of CO emission lines in the outer filaments and to study the CO(2–1)/CO(1–0) line ratio, we observed seven regions of interest again with the 30m telescope in both CO(1–0) and CO(2–1). The regions we observed were: the eastern filament, the horseshoe, the northern filament and a southern extension, all selected from H α emission line mapping. Molecular gas is detected in all the observed regions. This result confirms the large extent of the cold molecular gas filaments. We discuss the CO(2–1)/CO(1–0) ratios in the filaments. The eastern filament has optically thick gas, whereas further away, the line ratio increases close to values expected for a warmer optically thin medium. We also show CO(1–0) and CO(2–1) lines in 9 regions closer to the centre. The kinematics of the CO is studied here in more detail and confirms that it follows the motions of the warm H₂ gas found in the near-infrared. Finally, we searched for dense gas tracers around 3C84 and claim here the first detection of HCN(3–2).

Key words. Galaxies: cD, cooling flows, intergalactic medium, Galaxies: individual: NGC 1275

1. Introduction

Over the past decade X-ray observations have shown a lack of cool X-ray emitting gas in cooling flow clusters (e.g. Peterson et al 2003), and many feedback models have been proposed to explain the required energy injection into the intracluster medium (e.g. Binney & Tabor 1995; Omma & Binney 2004). At the same time, large amounts of molecular gas have been found in many Brightest Cluster Galaxies (BCG) (Edge 2001; Salomé & Combes 2003), providing evidence that some of the ICM may cool to very low temperatures. Detailed studies of this cold molecular gas reservoir are a complementary way to probe feedback processes.

The giant cD galaxy NGC 1275 is the central galaxy of the Perseus cluster (Abell 426) and lies at a redshift of 0.01756. At this distance, 1'' is 350 pc ($H_0 = 71$ km/s/Mpc, $\Omega_M=0.27$, $\Omega_\lambda=0.73$). This object is famous for the huge filamentary structure detected in the optical (Hu et al., 1983, Conselice et al. 2001). These bright H α emitting filaments are known to be

directly/indirectly associated with cooling cores (Crawford et al., 1999; Edwards et al., 2007). We have shown previously (Salomé et al., 2006; hereafter S06) that the molecular gas is also detected in CO(2–1) emission in the centre of NGC 1275 with morphology and dynamics identical to that of the H α emission.

We present here the results of follow-up observations aimed at confirming the presence of cold gas associated with the optical filaments further out from the galaxy. We looked for CO(1–0) and CO(2–1) emission lines in 7 regions selected in the optical filaments. We also observed the central region at both 1.3 and 3mm with high sensitivity receivers. Section 2 describes the observations. Section 3 presents the results and discusses the spectra obtained in the different regions of interest. We then compare the CO results (morphology, kinematics, line ratios) with data at other wavelengths in section 4. Section 5 summarizes our conclusions.

2. Observations

The observations were made with the IRAM 30m telescope on Pico Veleta, Spain during two different runs in 2006. We used

Send offprint requests to: salome@iram.fr

* Based on observations carried out at the IRAM 30m telescope, with the help of IRAM members, Pico Veleta, Spain.

the wobbler switching mode with two 3mm and two 1.3mm receivers operating simultaneously. The beam throw was 4 arcmin. Receivers were tuned to the CO(1–0) and CO(2–1) emission lines, redshifted to the velocity of NGC 1275. Frequent pointings were done on 3C84, the radio source at the centre of NGC 1275. At 3mm, we used two 512×1 MHz filter-banks. This gives a total band of ~ 1300 km/s for the CO(1–0) line setup. In addition, we used the two 250×4 MHz resolution filter-banks for the 1.3mm receivers, providing a 1 GHz band width, for the 1.3mm receivers which also corresponds to a 1300 km/s bandwidth. The beams of the 30m telescope, at 3mm (113.282 GHz) and 1.3mm (226.559 GHz), are respectively $22''$ and $11''$.

Regions close to the centre were very quickly detected (in 10–20 min), while the more distant regions required more time (~ 2 hours). The signals are expressed here in main beam brightness temperatures. The main-beam efficiency of the 30m telescope is the ratio of the antenna temperature to the main beam temperature: $T_A^*/T_{mb} = B_{eff}/F_{eff}$ with the ratio of the beam efficiency to the forward efficiency being: $B_{eff}/F_{eff} = 0.75/0.95$ at 3mm and $0.52/0.91$ at 1.3mm (cf IRAM-30m site <http://www.iram.es/>).

The data were calibrated with the MIRA software and reduced with the CLASS90 package. Spiky channels and bad scans were dropped and linear baselines were subtracted for each spectrum. After averaging all the spectra for each line at each position, the data were Hanning smoothed to a 42 km/s resolution.

The data are summarized in Tables 1 and 2. The CO(2–1) lines of the filaments use the present observations and the data obtained with HERA (S06): the CO(2–1) spectra were convolved with the beam pattern at 3mm to compare the CO(1–0) and CO(2–1) temperatures.

3. Results

We detected CO in all the regions observed inside the H α filaments. Offsets are relative to the 3C84 position : RA 03:19:48.15, Dec 41:30:42.1 (J2000). In the central region (indicated as centre 1 to 9 in Fig 1 and Table 2), the 3mm data suffered from baselines instabilities due to the strong continuum of 3C84. The 3mm spectra shown on the left hand side of Fig 4 are affected by those baseline ripples. The 1.3mm data, not affected by baseline ripples give a more reliable idea of the line shape. Nevertheless *CO lines are detected in all regions except the region outside the H α filaments*. This is the region named test, which has no H α emitting counterpart. Our earlier HERA map (S06) showed a hint of a detection at this place, but this was not confirmed by the new observations.

In order to compute the molecular gas content from the integrated CO intensity I_{CO} (K.km/s), we used

$$I_{CO} = \int T_{mb}(CO) dV, \quad (1)$$

where $T_{mb}(CO)$ is the main beam antenna brightness temperature, obtained with the CO emission line and dV is the line

width. We then adopted the standard Milky Way conversion factor commonly used for $N(H_2)$ estimates:

$$N(H_2) = 2.3 \cdot 10^{20} I_{CO} \text{ (molecules/cm}^2\text{)}. \quad (2)$$

From this equation the mass of molecular hydrogen, contained in one beam is:

$$M_{gas} (M_{\odot}) = 1.36 \times 2.95 \cdot 10^{-19} I_{CO} \theta^2 D^2 \frac{N(H_2)}{I_{CO}}, \quad (3)$$

I_{CO} is the integrated intensity in K km/s, θ is the beamsize of the telescope in arcsec, and D is the distance of the galaxy, taken to be 72.6 Mpc. We also included a factor 1.36 to take into account the He contribution to the gas mass.

3.1. The filaments

We describe below the regions selected from our HERA map (see S06). These regions were chosen to be distant from the East-West filament seen in CO(2–1) and known for their peculiar optical morphology. The first aim was to confirm the CO detections far away from the central galaxy. The regions called Off 1, Off 2 and Pos 2 trace the northern and southern filaments visible in H α up to a projected distance of 25 kpc north and south of the galaxy. Pos 11 is centred on a looped-back filament seen in optical emission lines that may trace uplifted gas behind a rising cold gas bubble inside the hot intracluster medium (Fabian et al., 2003; Hatch et al., 2006). Finally, closer to the centre, East and Off 3, are two fields in the eastern filament. The East region includes a young star cluster (Shields and Filipenko, 1990).

We now compare the velocity shift of our CO detections with the velocities of the warm (2000 K) H_2 gas detected by Hatch et al., (2005) and the hot (10^4 K) optical line emitting gas measured by Hatch et al. (2006).

The eastern filament: refers to positions East and Off 3, at about 8 kpc from the galaxy's centre. It corresponds to regions named A, B, C and D in Hatch et al. (2005). The CO emission lines are centred at -100 km/s relative to the systemic velocity. This blueshift is the same as the velocity found for the P α , Bry and H_2 $v=1-0$ S(1), S(2) and S(3) lines detected by the above mentioned authors.

The southern filament: refers to position Pos 2 at 25 kpc from the galaxy's centre. It corresponds to regions named SW1 and SW2 in Hatch et al. 2005. Here again, the CO emission is blueshifted relative to the nucleus, like the infrared H_2 tracers.

The horseshoe: refers to the position Pos 11, at least 25 kpc from the galaxy's centre. The CO(1–0) line is detected at the limit of the sensitivity reached. There is also a tentative detection of CO(2–1) line which disappears when merged with the HERA data, so this detection is not very strong. Nevertheless, the two emission lines have positive velocities (36 km/s and 120 km/s). This velocity range agrees with that from the infrared H_2 tracers by Hatch et al. (2005). It is also the same velocity shift as the hot H α emitting gas found by Hatch et al. (2006) in the loop of the horseshoe filament (see their Figure 6).

The northern filament: This region refers to the position Off 2, at about 25 kpc from the galaxy centre. The H α emitting

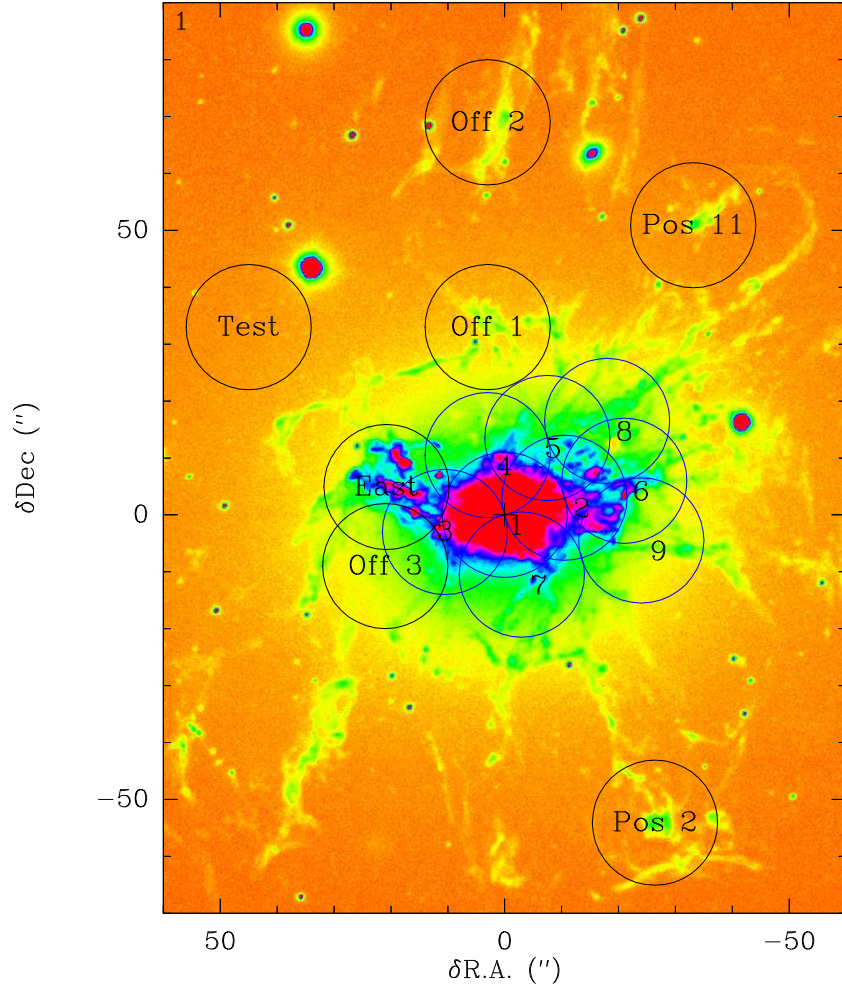


Fig. 1. $H\alpha$ image of the filament system in NGC1275 (Conselice et al., 2001). Overlaid are the regions re-observed with the 30m telescope. The circles represent the beam size at 3mm.

gas has a velocity range between +6 and +41 km/s relative to the systematic velocity. This is similar to the velocity of the CO line.

The tangential filament: This region refers to position Off 1, at least 12.3 kpc from the galaxy centre. It corresponds to a region inside the tangential filament (slit 5) of Hatch et al. 2006. The CO velocity is not well defined here as it is not consistent between the 3mm and the 1.3mm data. However, there is a hint of a two-component velocity structure, at ± 100 km/s. This is consistent with the $H\alpha$ velocity found in the same region (distance between ~ 15 and ~ 20 kpc in Fig. 7 of Hatch et al., 2006).

The test region: A hint of a CO(2–1) detection was present in the S06 HERA data, in a region that corresponds to no $H\alpha$ filament. We re-observed this region and found no CO(1–0) or CO(2–1) emission (i.e. $M_{\text{gas}} < 10^8 M_{\odot}$). We conclude that there is no, or very little, cold gas outside the $H\alpha$ filaments.

3.2. The central region

We observed 9 regions to map the CO emission close to 3C84. We present here a fully sampled CO(1–0) map of about $50'' \times 50''$ with a spatial resolution of $22''$. The CO(2–1) map does

not fully sample the same region but has a better resolution of $11''$. All the results are described in more detail in Table 2 and Figs 3 and 4. In the central regions the CO(1–0) and CO(2–1) line profiles are similar. The CO(2–1) line fluxes, when not convolved with the CO(1–0) beam, are 4 times larger than the CO(1–0) fluxes. So within the uncertainties, this is in agreement with an optically thick cold gas. After convolution, all the ratios are close to one. Some regions have a ratio greater than one, but as mentioned before, the CO(1–0) lines are affected by baseline ripples close to 3C84. The main beam brightness temperatures in CO(1–0) are thus very likely under-estimated in this region.

3.3. Detection of HCN(3–2)

We searched for HCN(1–0), HCN(2–1) and HCN(3–2) emission lines in the centre of NGC 1275. The observations at low frequency were corrupted by strong baseline ripples due to the strong continuum source 3C84. So we focus on the HCN(3–2) observations at 261 GHz, observed in average weather conditions. The spectrum presented in Fig 5 is the average of data taken during a first run with the two receivers detecting two polarisations (A230, B230) and during a second run with the two

Table 1. Results of the observations.

Position	Offsets [$\prime\prime \times \prime\prime$]	Line	T_{mb} [mK]	Velocity [km/s]	Width [km/s]	I_{CO} [K.km/s]	M_{gas} [$10^8 M_{\odot}$]	T_{21}/T_{10}
Off1	[3, 33]	CO(1-0)	2 ± 1.0	33.3 ± 37.1	237.6 ± 59.8	0.5 ± 0.1	1.1	
Off1	[3, 33]	CO(2-1)	5.3 ± 1.8	-55.2 ± 26	275 ± 47.7	1.5 ± 0.3		
Off1	[3, 33]	CO(2-1)	4.7 ± 0.8	-18.4 ± 12.9	247.1 ± 26.7	1.2 ± 0.1		2.4
Off2	[3, 69]	CO(1-0)	2.5 ± 0.6	49 ± 13.4	128.5 ± 31.1	0.3 ± 0.1	0.8	
Off2	[3, 69]	CO(2-1)	7.8 ± 2.3	-21.8 ± 20.7	210.6 ± 43	1.8 ± 0.3		
Off2	[3, 69]	CO(2-1)	4 ± 1.2	-29.3 ± 25	187.3 ± 73.9	0.8 ± 0.2		1.6
Off3	[21, -9]	CO(1-0)	15.2 ± 2.9	-91.2 ± 8.4	93 ± 16.9	1.5 ± 0.3	3.5	
Off3	[21, -9]	CO(2-1)	9.4 ± 3.1	-88.1 ± 24.7	276.6 ± 48.6	2.77 ± 0.5		
Off3	[21, -9]	CO(2-1)	8.2 ± 0.9	-62.8 ± 6.5	153.8 ± 17.7	1.34 ± 0.1		0.5
Pos11	[-45, 51]	CO(1-0)	1.5 ± 0.7	65 ± 32.2	272.6 ± 119.9	0.44 ± 0.13	1	
Pos11	[-45, 51]	CO(2-1)	3 ± 1.5	55 ± 21.5	96.2 ± 45.6	0.31 ± 0.13		2*
Pos11	[-45, 51]	CO(2-1)	$\leq 3 \times 1.3$	-	-	-		
Pos2	[-45, -51]	CO(1-0)	1.9 ± 0.9	-47.8 ± 25.7	116.9 ± 48.1	0.2 ± 0.1	0.5	
Pos2	[-45, -51]	CO(2-1)	3.8 ± 1.6	-65.4 ± 27.9	205 ± 53.2	0.8 ± 0.2		
Pos2	[-45, -51]	CO(2-1)	2.3 ± 1.0	-64.4 ± 23.2	140.6 ± 51.1	0.3 ± 0.1		1.2
East	[27, 3]	CO(1-0)	23.4 ± 4.5	-109.1 ± 9.1	106.2 ± 20.1	2.6 ± 0.5	6.2	
East	[27, 3]	CO(2-1)	36.2 ± 4.5	-84.3 ± 6.4	124.3 ± 15.9	4.7 ± 0.5		
East	[27, 3]	CO(2-1)	13.4 ± 1.0	-71.4 ± 3.7	127.5 ± 9.9	1.8 ± 0.1		0.6
Test	[45, 33]	CO10	$\leq 3 \times 1.6$	-	-	-	-	
Test	[45, 33]	CO21	$\leq 3 \times 5.9$	-	-	-	-	

*Estimated without the HERA data. Note that the CO(1-0) could be half the value in the table here, see spectra on Fig 2.

other receivers C270 and D270. The signal appears marginally in both data sets and even better in the averaged spectrum. So we claim a detection of HCN(3-2). The S/N ratio on the integrated line is 6.

The HCN molecule has a large dipole moment that requires $n(H_2) > 10^4 \text{ cm}^{-3}$ for significant excitation. This tracer of dense gas regions is thus considered as an indicator of star formation activity (Gao & Solomon, 2004). We computed the apparent CO and HCN luminosities (using equation 1 from Downes et al., 1999) from the integrated line flux measured in CO(1-0) and HCN(3-2). We assumed a HCN(3-2)/HCN(1-0) ratio close to one. At densities higher than a few 10^4 cm^{-3} for a temperature higher than 40-50 K, radiative transfer models predict a ratio larger than ~ 0.25 . We found $L'_{CO} = 5 \times 10^8 \text{ K km/s pc}^2$ and $L'_{HCN} = 5 \times 10^7 \text{ K km/s pc}^2$. When compared to the $L_{FIR} - L'_{CO}$ and $L_{FIR} - L'_{HCN}$ relations as described by Solomon et al. (1992, 1997), our measurements fall in the normal spiral galaxies range and independently predict an L_{FIR} of $2 \times 10^{10} L_{\odot}$. Lester et al., (1995) estimated the thermal FIR emission to be $10^{11} L_{\odot}$, with the approximation that only 20% of the total luminosity was non-thermal. This is an order of magnitude higher than the L_{FIR} predicted here. So either the contribution of the synchrotron emission is larger than expected or there is an excess of FIR emission in NGC1275 compared to the well-known $L_{FIR} - L'_{HCN}$ relation for star forming galaxies.

3.4. Molecular gas from the High Velocity Component

NGC1275 is surrounded by some star formation regions, with young star clusters, that could be formed in a merger but also in the cooling flow (see S06). Some are associated with the High Velocity System (HVS) at 8200 km/s, which appears in absorp-

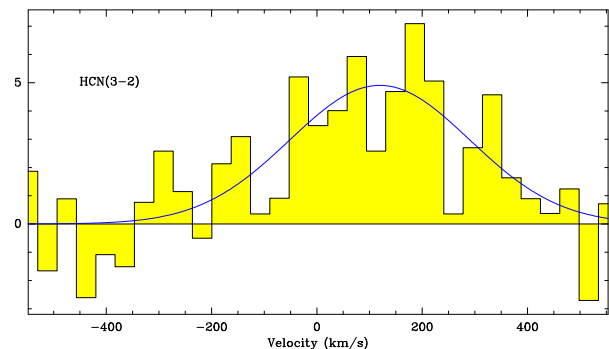


Fig. 5. HCN(3-2) emission lines in T_{mb} (mK), observed with the 30m telescope (290 min). A gaussian fit gives I_{HCN} 2.1 K.km/s with a peak temperature of 5 mK, a velocity of 120 km/s and a linewidth of 400 km/s. The rms is 1.6 mK with a mean T_{sys} of 445 K. The channel width is 36 km/s.

tion in front of the optical emission of NGC 1275 (Gillmon et al., 2004). No stellar component is detected, even in the near-infrared, corresponding to the HVS, which could be a gas-rich disrupted dwarf, or tidal debris, as proposed by Hu et al (1983).

We searched for CO emission at 8280 km s^{-1} on one position in the HVS (centred on 3C84's position). The results are shown in Fig 6. There is no clear detection but a hint of CO(1-0) emission. The line intensity we derive is up to a maximum of the order of 0.4 K.km/s which corresponds to $\leq 10^8 M_{\odot}$ of cold gas. So even if interacting with the ambient medium closely surrounding NGC 1275, the HVS contains a very small amount of cold gas. This mass is comparable or less than what is found in the cold filaments around the cD galaxy. Therefore, if the

Table 2. Results of the observations.

Position	Offsets [$'' \times ''$]	Line	T_{mb} [mK]	Velocity [km/s]	Width [km/s]	I_{CO} [K.km/s]	M_{gas} [$10^8 M_{\odot}$]	T_{21}/T_{10}
centre1	[0, 0]	CO(1-0)	15.2 ± 4.2	-70.2 ± 22.8	333 ± 69.1	5.4 ± 0.8	12.6	
centre1	[0, 0]	CO(2-1)	76 ± 4.6	-25 ± 4.8	301 ± 11.5	24.3 ± 0.8		
centre1	[0, 0]	CO(2-1)	26.7 ± 1.6	-41.2 ± 4.5	277.9 ± 10.9	7.9 ± 0.26		1.7
centre2	[-11, 3]	CO(1-0)	26.7 ± 5.6	-74.8 ± 16.4	238.6 ± 41.3	6.8 ± 0.9	15.8	
centre2	[-11, 3]	CO(2-1)	83.7 ± 17.2	-99.7 ± 14.8	231.7 ± 34.6	20.6 ± 2.6		
centre2	[-11, 3]	CO(2-1)	31.1 ± 1.2	-63.8 ± 2.9	257.6 ± 6.7	8.5 ± 0.2		1.2
centre3	[11, -3]	CO(1-0)	10.3 ± 5.1	-60.4 ± 81.2	340.3 ± 216.2	3.7 ± 1.4	8.7	
centre3	[11, -3]	CO(2-1)	29.7 ± 10.2	9.4 ± 29.1	340.2 ± 69.2	10.7 ± 1.9		
centre3	[11, -3]	CO(2-1)	16 ± 1.3	-45.1 ± 5.9	248.4 ± 15.4	4.2 ± 0.2		1.6
centre4	[3, 11]	CO(1-0)	26.4 ± 8.4	-36.9 ± 13.4	83.1 ± 29.6	2.3 ± 0.8	5.4	
centre4	[3, 11]	CO(2-1)	18.7 ± 12.2	-61.5 ± 60.7	320.4 ± 97.8	6.4 ± 2.0		
centre4	[3, 11]	CO(2-1)	17 ± 1.1	-44.7 ± 4.9	271.2 ± 12.1	4.9 ± 0.2		0.6
centre5	[-8, 14]	CO(1-0)	22.9 ± 7.6	-74.5 ± 20.4	167.5 ± 43.3	4.1 ± 1.0	9.5	
centre5	[-8, 14]	CO(2-1)	33.2 ± 10.1	-76 ± 21.6	246 ± 50	8.7 ± 1.5		
centre5	[-8, 14]	CO(2-1)	23.8 ± 0.6	-61.3 ± 1.7	248.2 ± 4.2	6.3 ± 0.1		1.0
centre6	[-21, 6]	CO(1-0)	23.4 ± 4.3	-87.4 ± 11.5	191.3 ± 31.9	4.7 ± 0.6	11.1	
centre6	[-21, 6]	CO(2-1)	-14.8 ± 12.2	165.9 ± 68	247.3 ± 162.8	-3.9 ± 2.0		
centre6	[-21, 6]	CO(2-1)	24 ± 1.1	-65.4 ± 3.1	246.7 ± 7.1	6.3 ± 0.2		1
centre7	[-3, -11]	CO(1-0)	10 ± 8.2	-34.9 ± 79.2	441.4 ± 209.8	4.7 ± 1.8	11	
centre7	[-3, -11]	CO(2-1)	32.4 ± 7.6	-164.8 ± 12.8	117 ± 39.8	4.0 ± 1.0		
centre7	[-3, -11]	CO(2-1)	15.5 ± 1.1	-32.7 ± 5.6	277.4 ± 13.8	4.5 ± 0.2		1.6
centre8	[-18, 17]	CO(1-0)	14.1 ± 2.2	-82.9 ± 8.5	142.8 ± 16.2	2.1 ± 0.2	5	
centre8	[-18, 17]	CO(2-1)	-28.2 ± 6.2	121.1 ± 14.5	47.6 ± 28.2	-1.4 ± 0.5		
centre8	[-18, 17]	CO(2-1)	21.1 ± 1.1	-56.1 ± 3.5	241.4 ± 8.2	5.4 ± 0.2		1.5
centre9	[-24, -5]	CO(1-0)	16.2 ± 5.6	-149.5 ± 16.3	114.3 ± 36.4	2.0 ± 0.6	4.6	
centre9	[-24, -5]	CO(2-1)	-48.9 ± 18.4	55.2 ± 15.4	63.7 ± 33.1	-3.3 ± 1.4		
centre9	[-24, -5]	CO(2-1)	12.4 ± 1.0	-64.2 ± 5.9	275.1 ± 14.3	3.6 ± 0.2		0.8

HVS merges with the cD galaxy, it will not deposit a significant amount of cool gas.

4. Discussion

4.1. CO(2–1)/CO(1–0) line ratios

We have computed the CO(2–1)/CO(1–0) line ratios. The data at 1.3mm were combined with the HERA data described in S06. We then convolved the CO(2–1) data by the CO(1–0) beam size in order to make a meaningful comparison. We list, in Table 1, the CO(2–1)/CO(1–0) line ratios of the different regions observed. If we compare the main beam temperature in the CO(2–1) spectra with and without the 3mm beam shape convolution (central and right hand side column of Fig. 2), we can see that we have lost some signal by diluting the 1.3mm emission with a larger beam size. This means that the molecular gas emission is very likely to come from a region that is smaller than the 1.3mm beam size ($11''$).

At Pos 11, the tentative detection of CO(2–1) disappears when convolved to the CO(1–0) beam. Regions Off 2, Pos 2, Pos 11 and East show lower main beam temperatures at 1.3mm when we applied the 3mm beam convolution. Therefore, the emission from these positions probably comes from regions with an angular size less than $22''$ (the beam size at 3mm). Regions Off 1 and Off 3 do not show lower main beam temperatures when convolved with the 3mm beam and are therefore

probably extended by at least $22''$. We have recently confirmed this last result by mapping the eastern filament with the Plateau de Bure interferometer. This shows that the molecular gas lies in thin ($\leq 2''$) and elongated structures, exactly coincident with the H α filaments (Salomé et al., 2008).

After convolution to the same beam size, we find the CO(2–1)/CO(1–0) line brightness temperature ratio is close to one in regions East, Off3, Pos2 and close to 3C84. Such a ratio indicates optically thick CO(1-0) and CO(2-1) emission lines (Eckart et al., 1988). For regions farther out from the galaxy centre like Off2, the ratio is slightly larger than one. However, we sometimes find the line widths smaller in CO(1–0) than in CO(2–1). This means that the apparently high ratio could actually be closer to one if the line widths were constrained to be the same. Note that the Off1 emission-line ratio is about 2.5 while the line shapes are the same at 1.3mm and 3mm. So we see hints of higher CO(2–1)/CO(1–0) ratios at larger radius from the galaxy centre. This particular high ratio (larger than one) indicates optically thin emission (Goldsmith et al., 1999).

Closer to the centre, the strong 3C84 source produced baseline ripples that affected the 3mm line shapes. However, we estimated CO(2–1)/CO(1–0) line ratios close to one, in agreement with an optically thick cold gas (see Table 2).

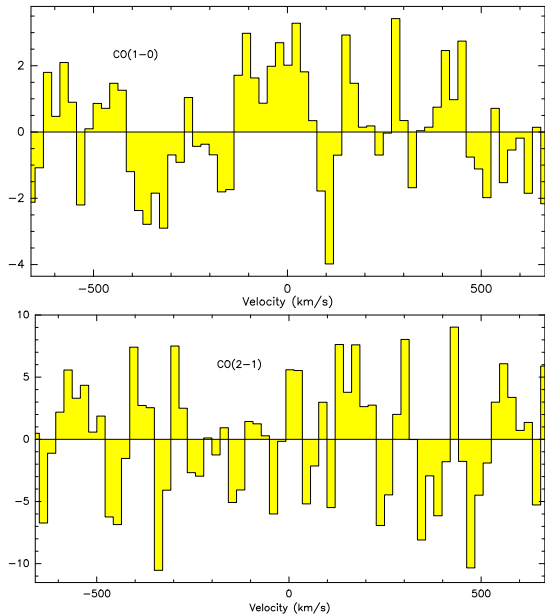


Fig. 6. Observations at 112.175 GHz (top) and 224.346 GHz (bottom), the CO(1–0) and CO(2–1) frequencies expected in the HVS restframe at 8280 km s^{-1} . No CO(2–1) is detected. There is a hint of detection in CO(1–0), with $I_{CO} = 0.4 \pm 0.1 \text{ K.km/s}$. This would give a mass of about $1 \times 10^8 M_{\odot}$. The channel width is 21 km/s.

4.2. Molecular gas reservoir and star formation

The scenario for the origin of the molecular gas we detect is that the cold gas accumulating towards the centre of the cluster gets dragged out with the bubbles and compressed in curved shocks, or flows back down around the borders of cavities. Feedback from the AGN not only heats the gas (negative feedback), but also compresses it in thin layers, that favors cooling and formation of molecular filaments (positive feedback) at a distance greater than 10 kpc (Revaz et al., 2008).

We expect no significant amounts of dust in the filaments, due to high sputtering rates. The question is then whether, in these conditions, there is still sufficient dust (which acts as a catalyst) to form molecules quickly. It may be that some dust from the ISM of NGC 1275 has been captured inside the up-lifted cooler gas and this is sufficient to catalyse the formation of molecules. Dust could also form in interstellar shocks, if present. The presence of dust grains at large radii would then help to form molecules in the outer filaments. A small quantity of dust grains is sufficient. We have proposed further observational investigations in order to constrain the amount of dust inside the filaments of NGC 1275.

For the assumed standard CO/H₂ conversion factor, the amount of molecular gas detected in the different regions observed varies from $7 \times 10^7 M_{\odot}$ to $8 \times 10^8 M_{\odot}$, which when added together gives a total mass of $1.3 \times 10^9 M_{\odot}$. These filaments therefore contain large quantities of cold molecular gas. The regions are also conspicuous in the emission lines of H α and [NII] but the optical line ratios are incompatible with young stars as the source of excitation as might be expected if stars were forming from the molecular gas. The excitation of these

lines is not coming from the AGN either, since it does not decrease with distance from the nucleus of NGC 1275 (Hatch et al 2006). The filaments are emitting extensively in UV and optical lines, much more than in X-rays, and a possible explanation for this is through heating by shocks at the interface between the relativistic jet plasma and the entrained gas at the exterior of the bubbles.

One of the most CO-rich regions is the eastern extension, which contains an unresolved ($< 1 \text{ kpc}$) young star cluster (Shields et al. 1990). The molecular gas mass of this region is greatly in excess of the mass of the star cluster and confirms a low star formation efficiency within the filaments (see also Salomé et al, 2008 for more details).

5. Conclusions

New CO(1–0) and CO(2–1) observations towards selected optical filaments around NGC 1275 confirm the presence of CO associated with the H α filaments. The gas kinematics are the same in CO and as in H α . We detect for the first time, a large amount of cold gas inside the outer filaments (a few $10^8 M_{\odot}$).

The excitation of the gas, derived from the comparison of CO(2–1) and CO(1–0) convolved to the same spatial resolution, indicates a range of densities are present. Optically thick emission is present close to the galaxy centre, whilst further out the emission could be optically thin.

We report a detection of HCN(3–2) emission in the centre, indicating high density gas. The association of the molecular gas with the H α filaments is consistent with the scenario in which cooling of the gas is taking place at large radii. This could happen in compressed hot gas at the border of the X-ray cavities. A detailed interpretation awaits specific simulations taking into account the cold, warm and hot gas phases.

Acknowledgements. IRAM is supported by INSU/CNRS (France), MPG (Germany) and IGN (Spain). RMJ acknowledges support by STFC and the Royal Society. We thank D. Downes for helpful comments and discussions.

References

- Binney, J., & Tabor, G., 1995, MNRAS, 276, 663
- Braine J., Duc P-A., Lisenfeld U. et al.: 2001, A&A 378, 51
- Brüggen M., & Kaiser C.R.: 2002, Nature 418, 301
- Carlson M.N., Holtzman J.A., Watson A.M. et al: 1998, AJ 115, 1778
- Cattaneo A., & Teyssier R.: 2007, 376, 1547
- Conselice, C.J., Gallagher, J.S., & Wise, R.F.G. 2001, AJ, 122, 2281
- Crawford, C. S., Allen, S. W., Ebeling, H., Edge, A. C., & Fabian, A. C., 1999, MNRAS, 306, 857
- Downes, D., Neri, R., Wiklind, T., Wilner, D.J., & Shaver, P.A., 1999, AJ, 513, L4
- Eckart, A., Downes, D., Genzel, R., Harris, A. I., Jaffe, D. T., & Wild, W., 1990, 348, 434
- Edge, A.C., 2001, MNRAS, 328, 762
- Edwards, L. O. V., Hudson, M. J., Balogh, M. L., & Smith, R. J., 2007, MNRAS, 319, 100
- Fabian, A.C., Sanders, J.S., Allen, S.W., et al. 2003, MNRAS, 344, L43
- Gao & Solomon, 2004, ApJ, 606, 271
- Gillmon K., Sanders J.S., & Fabian A.C., 2004, MNRAS 348, 159

- Goldsmith, P.F., & Langer, W.D., 1999, 517, 209
- Gonzalez-Martin O., Fabian A.C., & Sanders J.S.: 2006, MNRAS 367, 1132
- Hatch, N.A., Crawford, C.S., Fabian, A.C., & Johnstone, R.M.J, 2005, MNRAS, 358, 765
- Hatch N.A., Craxford C.S., Johnstone R.M., & Fabian A.C.: 2006, MNRAS 367, 433
- Hibbard J.E., & van Gorkom J.H.: 1996, AJ 111, 655
- Higdon S.J., Higdon J.L., & Marshall J.: 2006, ApJ 640, 768
- Hu E.M., Cowie L.L., Kaaret P., et al: 1983, ApJ 275, L27
- Inoue, M.Y., Kamenno, S., Kawabe, R., Inoue, M., Hasegawa, T., & Tanaka, M., 1996, AJ, 111, 1852
- Lester, D. F., Zink, E. C., Doppmann, G. W., Gaffney, N. I., Harvey, P. M., Smith, B. J., & Malkan, M., 1995, ApJ, 439, 185
- McNamara, B.R., O'Connell, R.W., & Sarazin, C.L, 1996, AJ, 112, 91
- Omma H., & Binney J., 2004, MNRAS, 350L, 13
- Revaz Y., Combes F., & Salomé P., 2008, A&A
- Salomé, P. & Combes, F., 2003, A&A, 412, 657
- Salomé, P. & Combes, F., 2004, A&A, 415, L1
- Salomé, P., Combes, F., Edge, A.C., et al., 2006, 454, 437
- Salomé, P., Revaz, Y., Combes, F., Pety, J., Downes, D., Edge, A.C., & Fabian, A.C., 2008, A&A (submitted)
- Shields, J.C. & Filippenko, A.V., 1990, ApJ, 353, L6
- Sijacki D., & Springel V.: 2006, MNRAS 366, 397
- Solomon, P.M., Downes, D., & Radford, S.J.E., 1992, ApJ, 387, L55
- Solomon, P.M., Downes, D., Radford, S.J.E., & Barrett, J.W., 1997, ApJ, 478, 144
- Xu C.K., Lu N., Condon J.J. et al: 2003, ApJ 595, 665
- Wilman, R. J., Edge, A. C., & Johnstone, R.M., 2005, MNRAS, 359, 755

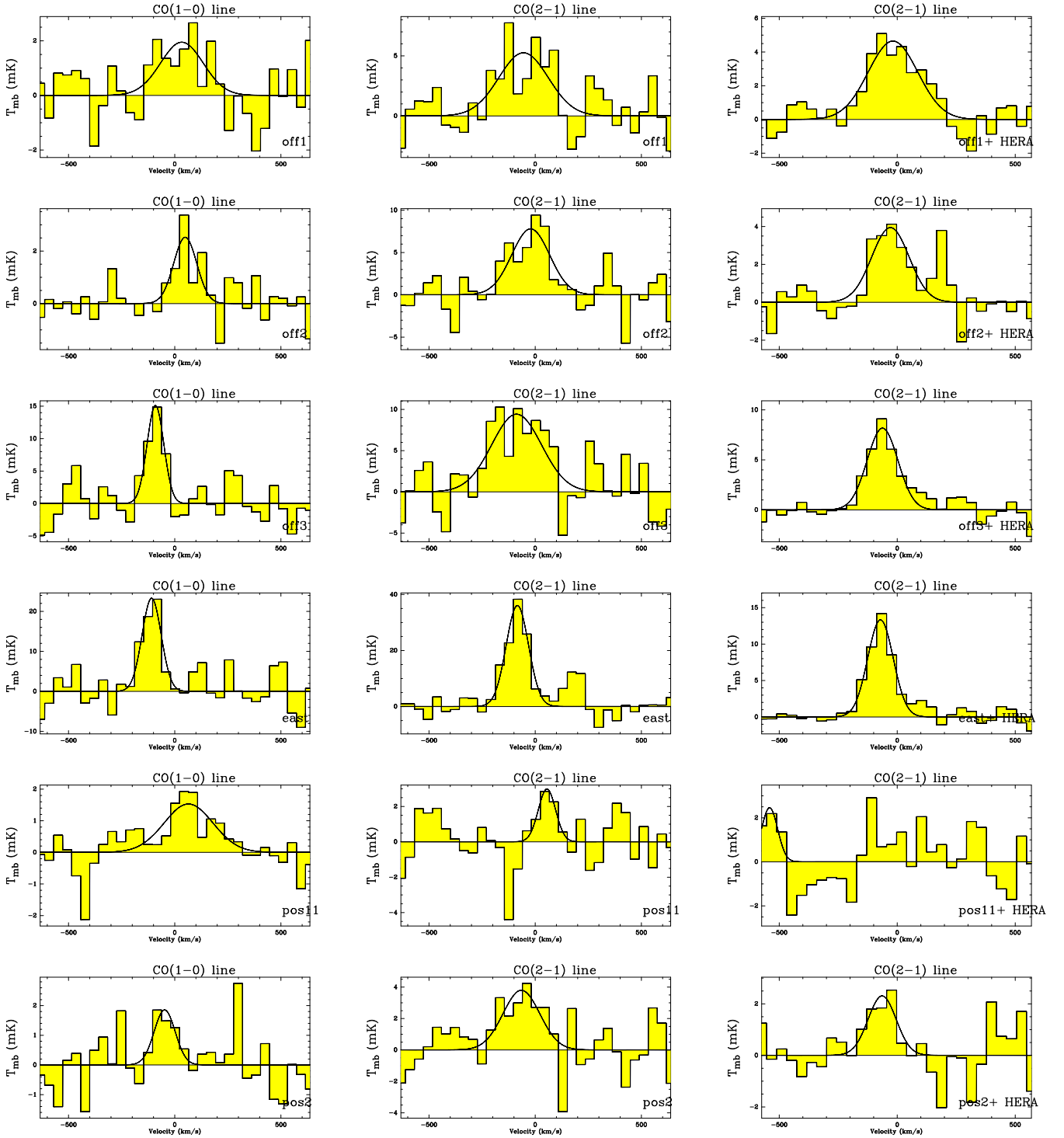


Fig. 2. CO(1–0) and CO(2–1) spectra obtained at all the positions observed as indicated at lower right in each diagram. The channel width is 42 km/s. On the left hand side are the CO(1–0) lines detected with the a100 and b100 receivers. In the middle are the results obtained for the CO(2–1) line with the A230 and B230 receivers. On the right hand side are the CO(2–1) lines computed with both A230 and B230 merged with previous HERA data and smoothed to the 3mm beam size.

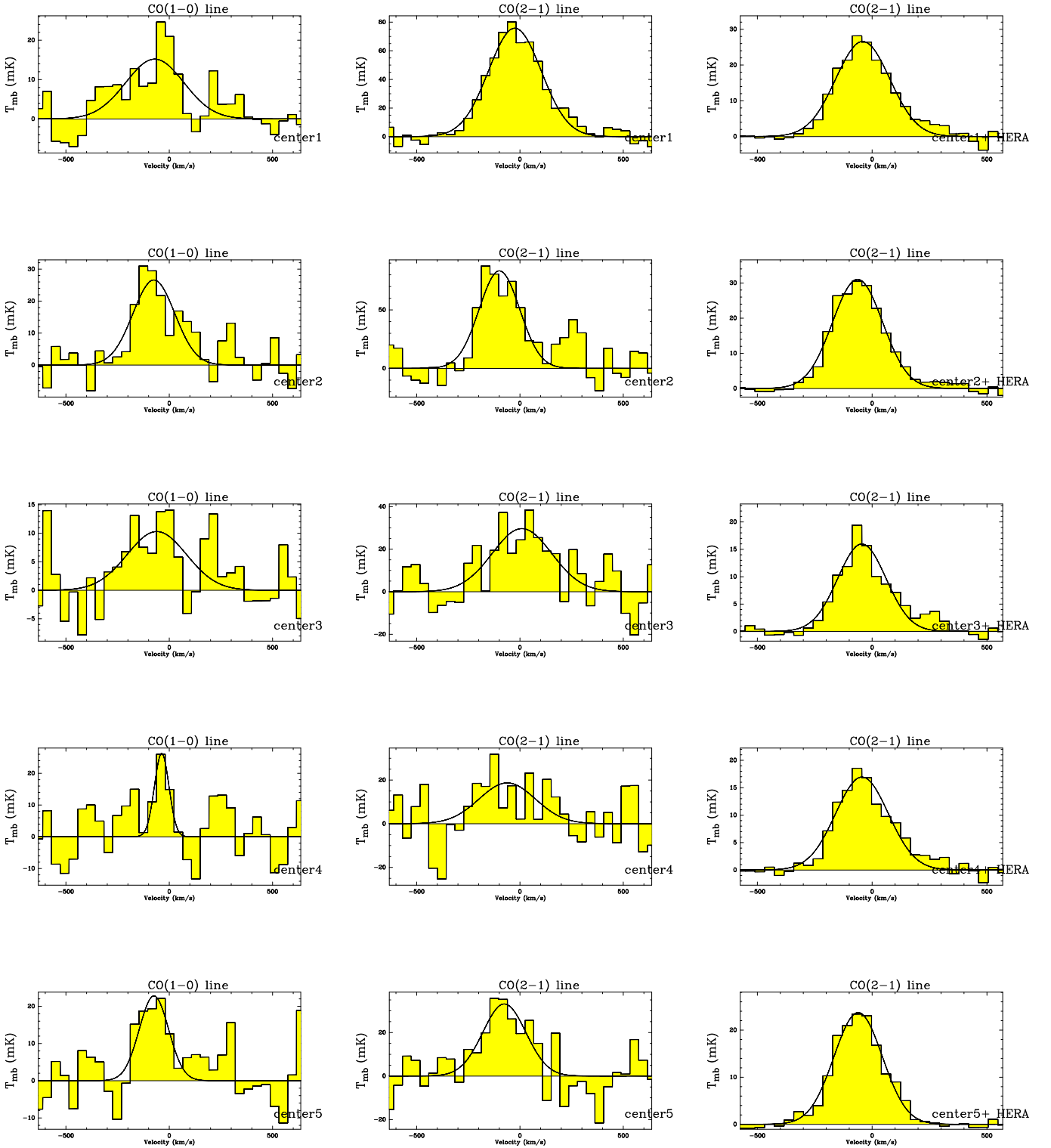


Fig. 3. CO(1-0) and CO(2-1) spectra obtained at all the positions near the centre of the galaxy as labeled in the lower right of each diagram. The channel width is 42 km/s, see Table 2.

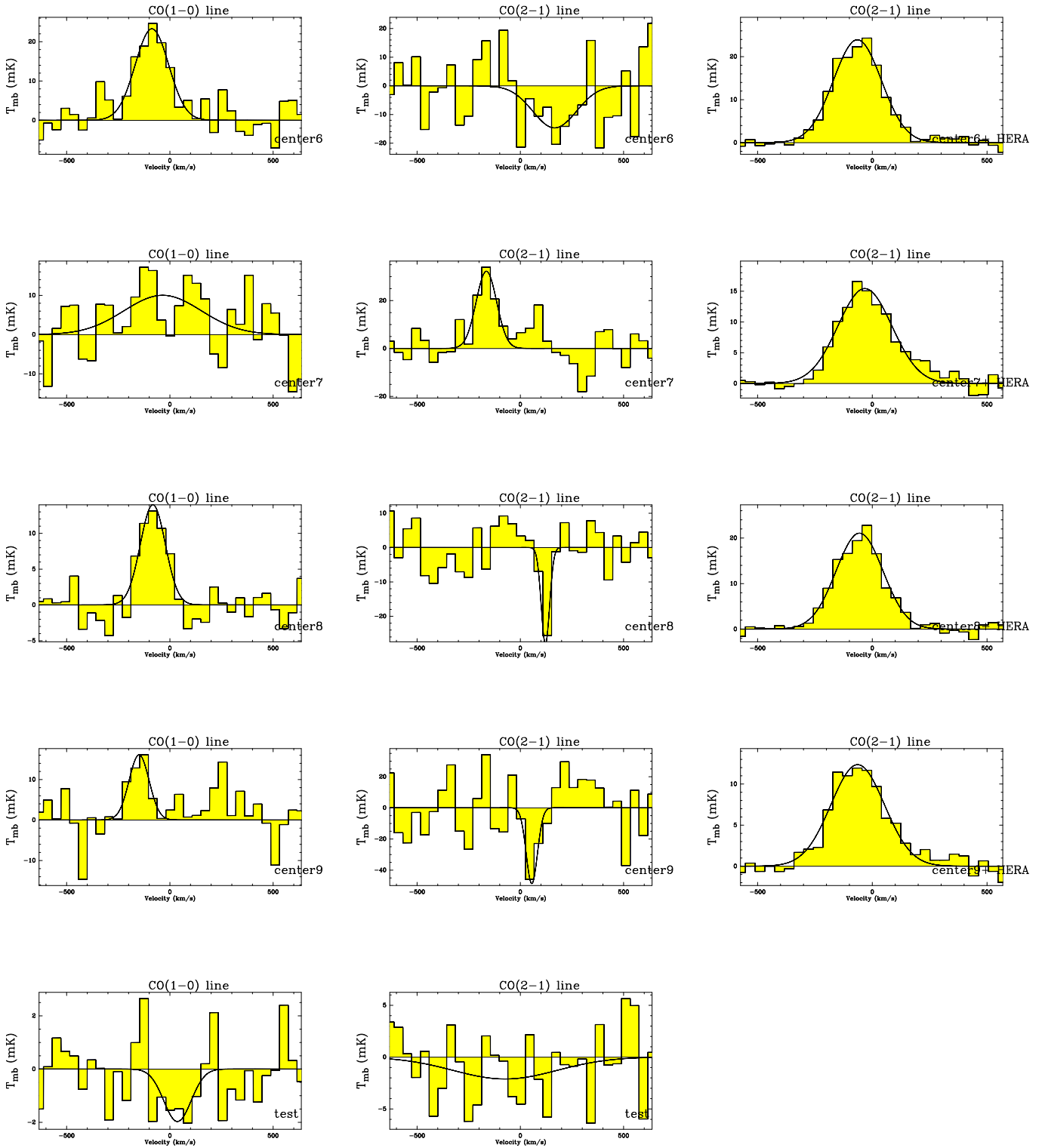


Fig. 4. CO(1-0) and CO(2-1) spectra obtained at all the positions near the centre of the galaxy as labeled in the lower right of each diagram. The channel width is 42 km/s, see Table 2.